The Vertical Structure of Temperature in the Tropics: Different Flavors of El Niño

KEVIN E. TRENBERTH AND LESLEY SMITH

National Center for Atmospheric Research,* Boulder, Colorado

ABSTRACT

To explore the vertical coherence of the vertical temperature structure in the atmosphere, an analysis is performed of the full three-dimensional spatial structure of the temperature field monthly mean anomalies from the 40-yr ECMWF Re-Analysis (ERA-40) for a core region of the Tropics from 30°N to 30°S, with results projected globally. The focus is on the first three empirical orthogonal functions (EOFs), two of which have primary relationships to El Niño–Southern Oscillation (ENSO) and feature rather different vertical structures. The second (EOF-2) also has a weak ENSO signature but a very complex vertical structure and reflects mainly nonlinear trends, some real but also some in large part spurious and associated with problems in assimilating satellite data. The dominant pattern (EOF-1) in its positive sign features highly coherent zonal mean warming throughout the tropical troposphere from 30°N to 30°S that increases in magnitude with height to 300 hPa, drops to zero about 100 hPa at the tropopause, and has reverse sign to 30 hPa with peak negative values at 70 hPa. Spatially at low levels it shows warmth throughout most of the Tropics although with weak or slightly opposite sign in the western tropical Pacific and a strong reversed sign in the Pacific subtropics. Coherent wave structures below 700 hPa at higher latitudes cancel out in the zonal mean. However, the structure becomes more zonal above about 700 hPa and features off-equatorial maxima straddling the equator in the eastern Pacific in the upper troposphere with opposite sign at 100 hPa, as a signature of a forced Rossby wave. The corresponding sea level pressure pattern is similar to but more focused in equatorial regions than the Southern Oscillation pattern. The time series highlights the 1997/98 El Niño along with those in 1982/83 and 1986/87, and the 1988/89 La Niña, and correlates strongly with global mean surface temperatures. Missing, however, is the prolonged sequence of three successive El Niño events in the early 1990s, which are highlighted in EOF-3 as part of a mainly lower-frequency decadal variation that features modest zonal mean warming below 700 hPa, cooling from 700 to 300 hPa, and warming above 300 hPa, peaking at 100 hPa and extending from 40°N to 50°S. Spatially at the surface this pattern is dominated by Southern Oscillation wave-1 structures throughout the Tropics and especially the subtropics. The regional temperature structures are coherent throughout the troposphere, with strongest values in the Pacific and extending well into the extratropics, with a sign reversal at and above 100 hPa. Strong Rossby wave signatures are featured in the troposphere with a distinctive quadrupole pattern that reverses at 100 hPa. The vertical coherence of all patterns suggests that they should be apparent in broad-layer satellite temperature records but that stratospheric anomalies are not independent. The quite different three-dimensional structure of these different patterns highlights the need to consider the full structure outside of the Pacific and at all vertical levels in accounting for impacts of ENSO, and how they relate to the global mean.

---

1. Introduction

A central issue in recent debates about climate change has been the relationship between changes in surface temperature versus those in the free atmosphere. As the climate warms, climate models tend to amplify changes in temperature with height in the Tropics, largely following the moist-adiabatic lapse rate, signaling the dominance of moist convection for determining the lapse rate in the tropical troposphere. For a given increase in surface temperature this means larger increases with height. For instance Santer et al. (2005) show how interannual variations of temperature in the tropical atmosphere indeed seem to feature amplification with height during El Niño events, as in model simulations, a finding with which the observed

behavior on decadal time scales and for trends is at odds. The evidence of very small trends in the free troposphere in radiosonde records in the Tropics (Free et al. 2005; Thorne et al. 2005) has recently been challenged by Sherwood et al. (2005), who show evidence of spurious downward daytime trends in temperature that is likely caused by improvements in sonde thermistors, which have become much smaller over time and are thus less affected by solar radiation effects. Randel and Wu (2006) have also found, by comparing satellite and sonde measurements, that even the quality-controlled sonde records (Free et al. 2004, 2005) still contain spurious, mostly downward, shifts likely associated with unaccounted for changes in sondes. Accordingly the evidence now suggests that the vertical temperature structure from observations should be reexamined.

This issue has been compounded by estimates of temperature changes from satellite sensors, notably those from the Microwave Sounder Unit (MSU), and after mid-1998, the follow-on Advanced MSU (AMSU; Christy et al. 2000, 2003; Mears et al. 2003). These have focused on the MSU channel-2 and channel-4 records, which provide estimates of temperature variations over very broad vertical layers. Channel 2 has a small surface signature, with the bulk of its signal coming from the troposphere, and about 15% coming from the lower stratosphere. Channel 4 has its entire signal from the lower stratosphere. Past use of channel 2 data as a proxy for tropospheric records, without accounting for the cooling in the lower stratosphere, has led to much lower estimates of tropospheric trends than is evidently the case when adjustments for the stratospheric influence are made (Fu et al. 2004a,b; Fu and Johanson 2004, 2005). The Fu technique is based on using linear regression of channels 2 and 4 to match radiosonde temperature estimates of tropospheric temperatures. Even though this technique has produced excellent statistical results, the implied vertical weighting function profile features some negative regions and some positive regions above the tropopause that have been criticized (Tett and Thorne 2004). For this technique to work, it has to take advantage of vertical coherence in temperature variations in the stratosphere in order to cancel out the various lobes in the statistical weighting function.

But what is the vertical coherence of temperature variations in the atmosphere? What are the predominant vertical structures that exist? Why does this technique evidently work? These are questions addressed in the current work. They cannot be addressed by satellite data, which have much too coarse vertical resolution for MSU data, and infrared channels are affected by clouds and are not all weather. The sonde data, as

noted above (also Seidel et al. 2004), are fraught with problems of all sorts, especially in regard to trends, and moreover they cover very little of the globe in the Tropics. We therefore use the European Centre for Medium Range Weather Forecasts (ECMWF) 40-plus years of reanalyses, referred to as the 40-yr ECMWF Re-Analysis (ERA-40). After 1978 these analyses are based on assimilation of all satellite data (infrared and microwave channels) plus radiosonde and aircraft data, as well as all surface data. As spurious discontinuities are present in the analyzed record at the end of 1978 when satellite data were introduced (Santer et al. 1999; Bromwich and Fogt 2004; Trenberth et al. 2005a), we use data only from 1979 on. Simmons et al. (2004) have evaluated the surface temperature record from ERA-40 and found generally excellent results with the notable exception of trends over Australia, where data availability compromised the record. Values are also somewhat unreliable in the 1990s, as contamination of the assimilated satellite sensor information by the Mount Pinatubo eruption in 1991 (Uppala et al. 2005; Trenberth et al. 2005a) affected the record. Hence we focus on monthly mean data to highlight the variability on all time scales in our analysis, and this should make the results more robust and minimize trend uncertainty influences.

Given the tropical focus and the inclusion of all months, it is not surprising that El Niño–Southern Oscillation (ENSO) emerges to dominate the structures, as Trenberth et al. (2005b) show that it is the dominant mode of variability globally, but it occurs not just in one pattern. Section 2 details the methods and data used, section 3 presents the results, and section 4 discusses these in the context of previous studies. The conclusions are given in section 5.

2. Methods and data

We began this study by forming monthly mean temperature anomalies relative to a climatology for 1979 to 2001 at each of the pressure levels in the ERA-40 archive. These include 11 levels from 1000 to 200 hPa as well as the 150-, 100-, 70-, 50-, 30-, and 10-hPa levels. We use the data at T63 resolution on a Gaussian grid, which corresponds to a grid of approximately 1.875°. A major task then is to find a way to distill this huge volume of data down into manageable amounts and the main tool for this is empirical orthogonal function (EOF) analysis. We have carried out several exploratory analyses. These include the following:

1) Global all months.
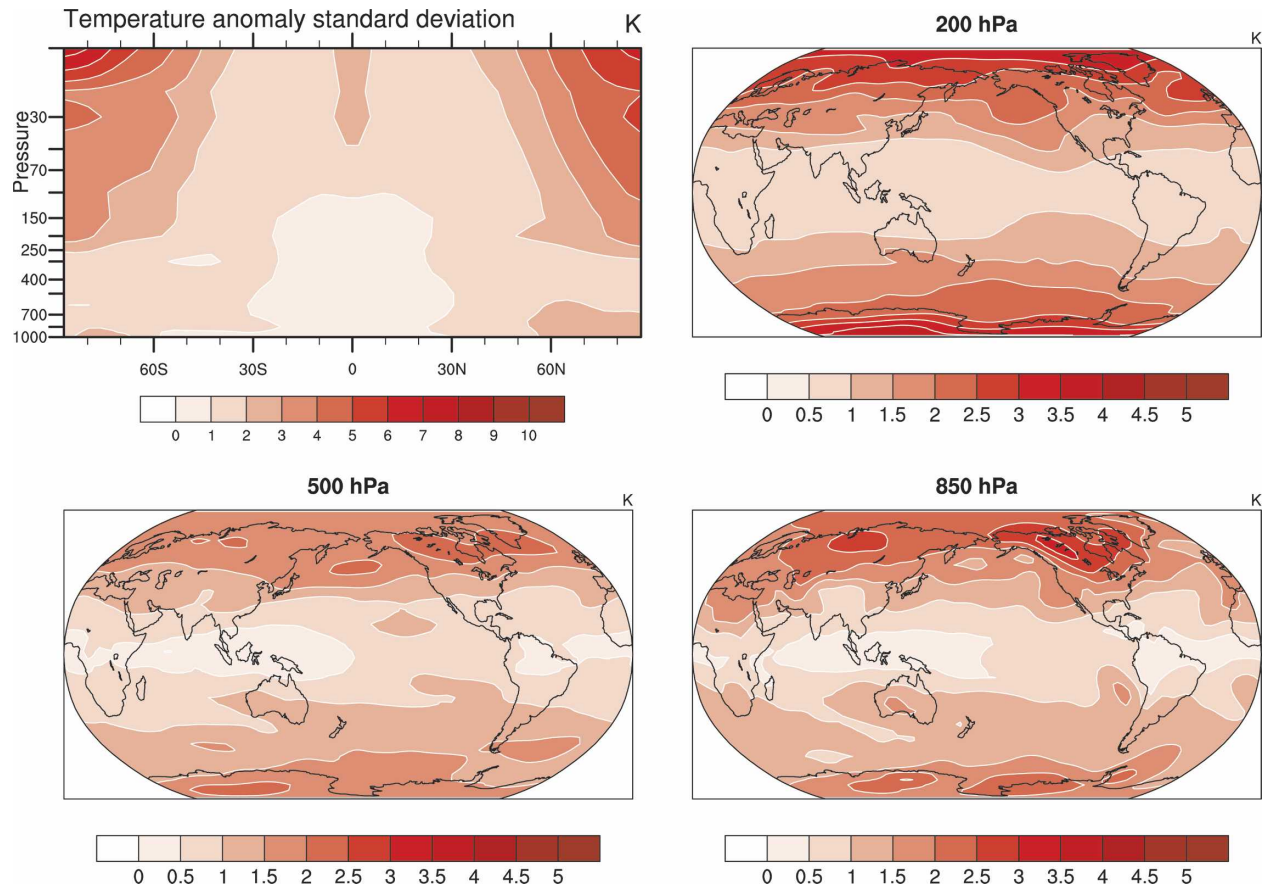2) Global northern summer/southern winter, in which

FIG. 1. Zonal mean of the monthly anomaly temperature standard deviations as a cross section, and standard deviations at 850, 500, and 200 hPa for 1979–2001.

anomalies for the five months of May–September (MJJAS) were included as independent values.

3) Global southern summer/northern winter in which the five monthly anomalies for November–March (NDJFM) were included.

4) Northern Hemisphere (NH) extratropics, north of 20°N, for both extended seasons.

5) Southern Hemisphere (SH) extratropics, south of 20°S, for both extended seasons.

6) Tropics from 30°N to 30°S for all months, as well as both NDJFM and MJJAS seasons.

The results are fascinating, but here we focus only on the results from the Tropics analysis for all months combined. In fact the global results are dominated by the Tropics, in spite of larger variance at higher latitudes, apparently because of the greater coherence of the tropical fluctuations. By confining the core analysis region to the Tropics we avoid possible contamination by seasonal influences from the northern annular mode (NAM), southern annular mode (SAM), and other primarily extratropical sources of variability (Trenberth et al. 2005b).

To perform the EOF analysis, nine levels were selected (1000, 850, 700, 600, 500, 400, 300, 200, and 100 hPa) as primary levels for the analysis and then results are projected onto all levels and the global domain using regression. The resolution is therefore 100 hPa except below 700 hPa where the 1000-hPa level is one sided (ideally we might use 800 and 900 hPa, but these are not available). We also performed analyses with other mixes of levels, and results do not change much, but, aside from mass weighting each level, this mix is the most uniform one available. The EOF analysis was performed with both the covariance matrix, thus feeding in the full temperature anomalies to the analysis, and the correlation matrix, which effectively normalizes each grid point by its standard deviation. The former emphasizes actual anomalies but tends therefore to weight results by variance, deemphasizing covariability.

Figure 1 presents the zonal mean of the standard deviations of monthly anomalies as a cross section and standard deviations at 850, 500, and 200 hPa. Variability is least in the Tropics, and patterns are predominantly zonally symmetric. Largest values occur over ex-

tratropical continents at low levels and generally increase with height to become a maximum at 10 hPa in the extratropical stratosphere of both hemispheres. Because we wish to emphasize covariability here, we choose to present only the results based on the correlation matrix. There are 23 yr of monthly anomalies—276 values—for which the correlation would need to exceed 0.12 to be significant at the 5% level if all values were independent. If only every third value is independent this increases to 0.20, and we regard this as a reasonable threshold for values worthy of further consideration.

3. Results

a. Indices of variability

The largest origin of tropical variability during the time period of interest is El Niño, and to depict the main variations we present in Fig. 2 the Niño-3.4 SST index as the area-average SST anomalies over 5°N–5°S, 170°–120°W and the Trans-Niño Index (TNI; Trenberth and Stepaniak 2001), which depicts normalized SST differences between the date line (Niño-4 region) and South American coast (Niño-1 + 2 region). These are essentially orthogonal and correspond to the two main descriptors of ENSO variability and evolution (Trenberth et al. 2002b). We also use the Southern Oscillation index (SOI). Of note during this period are the major El Niño events of 1982/83, 1986/87, 1991–95, and 1997/98 and with cold La Niña events in 1988/89 and 1999/2000. These events have strong signatures throughout the troposphere (e.g., Trenberth et al. 2002a). Also during this time (1979–2001), tropical SSTs as a whole experienced a warming trend of order 0.3°C, and so we use an estimate of the global mean surface temperature as an index. This is based upon the Climate Research Unit (CRU) of the University of East Anglia, Norwich, United Kingdom, land surface air temperatures and the U.K. Met Office's Hadley Centre SST analysis known as HADCRUT2v (Rayner et al. 2003; Jones and Moberg 2003).

Also potentially of relevance during this period were the El Chichōn and Mount Pinatubo volcanic eruptions. Late March and early April 1982 was the time of the El Chichōn volcanic eruptions that resulted in large quantities (7 million metric tonnes) of sulfur dioxide and 20 million metric tonnes of particulates into the lower stratosphere (Robock 2002) and in fact led to delayed recognition that the El Niño event was underway, as it masked the SST signal from satellites. It is smaller in size only to the Mount Pinatubo eruption,
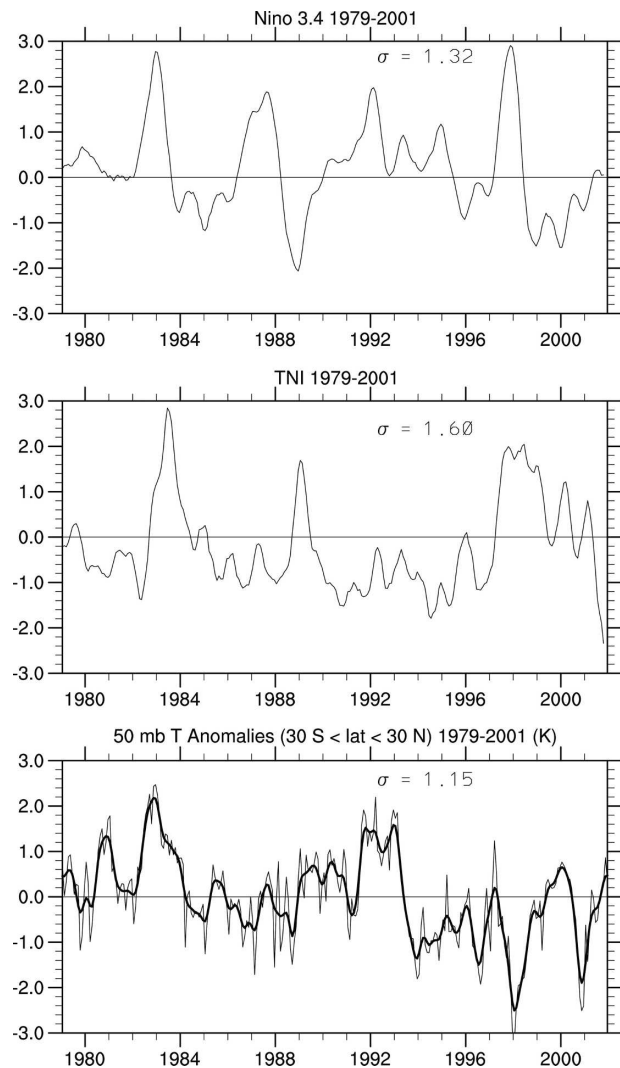

FIG. 2. Time series of indices of Niño-3.4 SSTs, TNI, and 50-hPa tropical temperatures. The heavy curve in the latter is filtered with a seven-point filter that emphasizes decadal variations. The values are departures from the 1961–90 climatology.

which developed after a series of smaller events into the main eruption in June 1991. Both eruptions led to extensive stratospheric aerosol for well over a year that first perturbed the infrared radiances used for monitoring temperatures, and second led to cooling of the climate system, but with a strong warming in the lower stratosphere. The latter is well tracked by MSU radiances. Therefore as well as the direct climate signature of such events, there may also be signs of aerosol contamination of the temperature record. To provide an index of this, we have simply averaged the 50-hPa temperature anomalies for 30°N to 30°S and smoothed it with a 1/24(1–3–5–6–5–3–1) filter, which highlights interannual variability (Fig. 2).
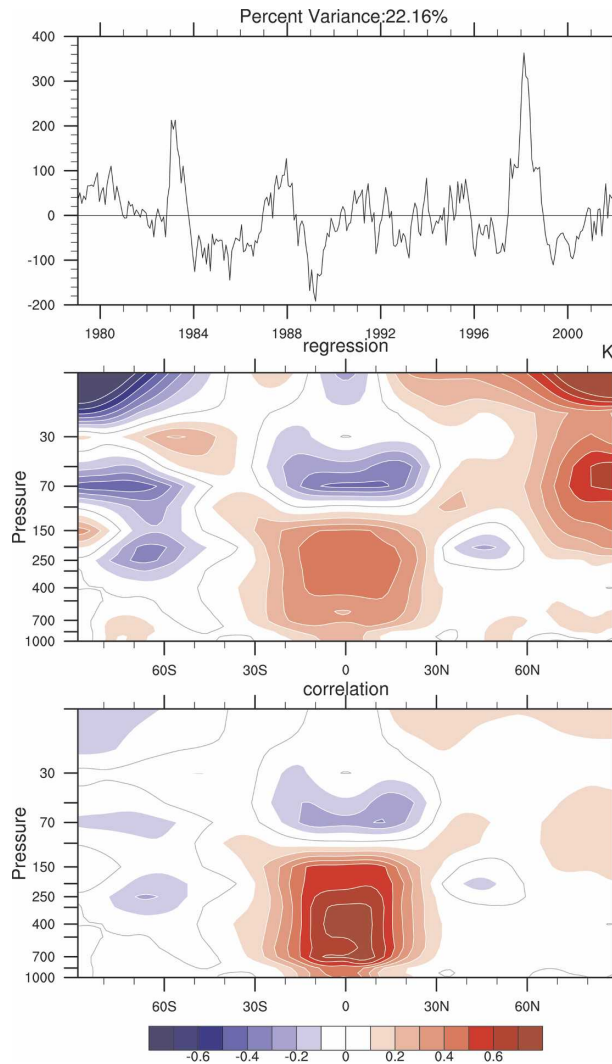
FIG. 3. For EOF-1: (top) principal component monthly anomaly time series for 1979–2001, and the (middle) regression and (bottom) correlation patterns for zonal mean temperature anomalies as latitude–pressure cross sections. The contour interval is (middle) 0.1 K per standard deviation and 0.1 for correlation.
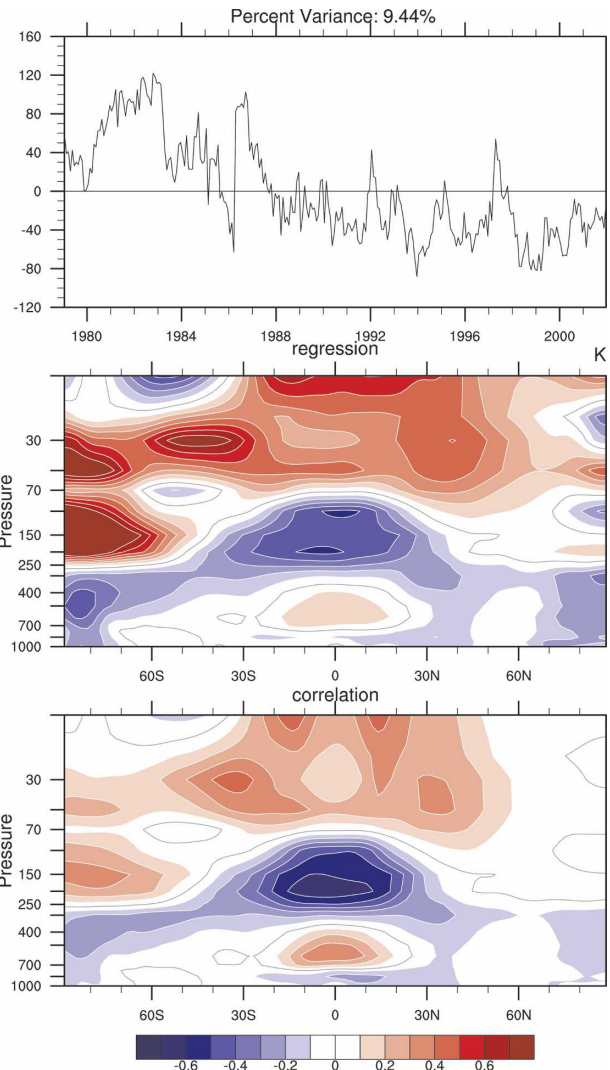

FIG. 4. For EOF-2: (top) principal component monthly anomaly time series, and the (middle) regression and (bottom) correlation patterns for zonal mean temperature anomalies as latitude–pressure cross sections. The contour interval is (middle) 0.1 K per standard deviation and 0.1 for correlation.

b. EOF results: Zonal mean vertical structure

We have chosen to feature three EOF results. In each of these we present the principal component time series, the zonal mean temperature anomaly structure (given by the covariance), and corresponding correlation (Figs. 3, 4, and 5). Then we also present the associated maps at several levels: 1000, 850, 700, 500, 300, 200, 100, and 50 hPa (Figs. 6, 7, and 8).

The first EOF, accounting for 22.2% of the tropical (30°N–30°S) temperature variance at the nine core levels, predominantly features the 1997/98 El Niño event in its time series (Fig. 3). Smaller representations are seen for the 1982/83 and 1986/87 El Niños, with the 1988/89 La Niña showing up also with opposite sign. There is nothing of consequence during the first half of the 1990s, however. Nevertheless, this EOF clearly features the main ENSO variability and its correlation with Niño-3.4 SST anomalies is 0.77, with Niño-3.4 leading by 3 and 4 months (0.58 at zero lag).

The second EOF (Fig. 4) accounts for 9.4% of the variance and features the 1982/83 El Niño but over a much more extended period, with a downward trend in this EOF after 1986/87, and persistently negative values after about 1990. The very high values include the time of the El Chichón eruption and its subsequent effects but seem to start in 1980. It is correlated with
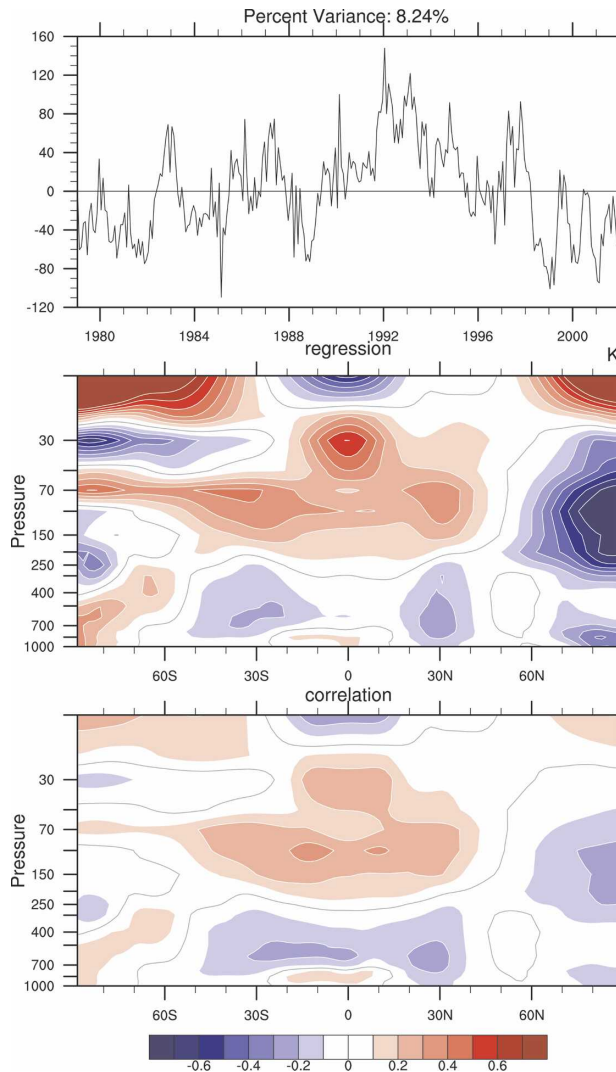
FIG. 5. For EOF-3: (top) principal component monthly anomaly time series, and the (middle) regression and (bottom) correlation patterns for zonal mean temperature anomalies as latitude–pressure cross sections. The contour interval is (middle) 0.1 K per standard deviation and 0.1 for correlation.

the monthly 50-hPa T (Fig. 2) 0.37, but only 0.30 with Niño-3.4.

The third EOF (Fig. 5) accounts for 8.2% of the variance. It is well separated from the next EOF (4.2%) and the previous one. The time series for this EOF features a marked contrast between the 1991–95 period with most of the rest of the record, although with a small 1997/98 signal. Curiously, the early 1990s is also the time of a prolonged and very unusual El Niño event (or series of three events in a row; Trenberth and Hoar 1996, 1997) and about the time of the Mount Pinatubo eruption. It is correlated at zero lag with Niño-3.4 SSTs at 0.59 and with the monthly SOI at 0.68.

These preliminary remarks, then, prompt a closer look as to the different flavor of the El Niño events and how much their character may have been influenced by the volcanic aerosol or trends. If we first examine the zonal mean temperature structures associated with each of these three EOFs (Figs. 3, 4, and 5), very different vertical structures in the Tropics are obvious. In each case we have chosen the sign convention to produce an El Niño–like warming at 1000 hPa in the Tropics for all three EOFs. However, for EOF-1, the warming intensifies with height to 300 hPa, drops to zero about the tropopause level at 100 hPa, and then features a reversal in sign in the lower stratosphere, mainly at 70 and 50 hPa. Correlations are very strong ($>$0.6) throughout the troposphere and the Tropics, and with only weak and statistically insignificant signatures at higher latitudes.

For EOF-2, the tropical East Pacific warming is not reflected in the zonal mean at 1000 hPa. Zonal mean warming is evident in the lower troposphere and peaks near 500 hPa but extends only to 370 hPa, although we shall see that the regional structure matters for this case. For the zonal mean, EOF-2 features pronounced tropical cooling from 350 to 100 hPa and then warming above 70 hPa. The correlations are strongest above 300 hPa and exceed –0.6 near 150 to 200 hPa and +0.3 in much of the stratosphere.

EOF-3 has only very shallow zonal mean warming in the Tropics, cooling from 400 to 700 hPa (peak negative correlation: –0.25 at 600 hPa) and then features peak warming in the upper troposphere above 300 hPa, that is strong at the tropopause level (correlation +0.3 at 100 hPa) to 30 hPa and extends well into the SH. The tropospheric signature extends from 45°N to 60°S and is not confined to the Tropics, and strong cooling is evident in the Arctic. These structures are very large scale and coherent.

For EOF-1 the main structure covers 30°N to 30°S and then seems to be associated with modest warming in the lower troposphere at higher latitudes of both hemispheres, but cooling aloft in the SH. For EOF-2, the upper-tropospheric cooling is coherent with regions at lower altitudes but higher latitudes in both hemispheres, and the lower stratospheric warming is also not just tropical but extends throughout the SH. For EOF-3 there is a strong signature of temperature anomaly of opposite sign in the NH extratropics, especially north of 60°N.

c. EOF results: Spatial structure

The maps of the corresponding structures at various levels (Figs. 6, 7, and 8) help clarify the nature of the zonal mean patterns. For EOF-1 the signature of the
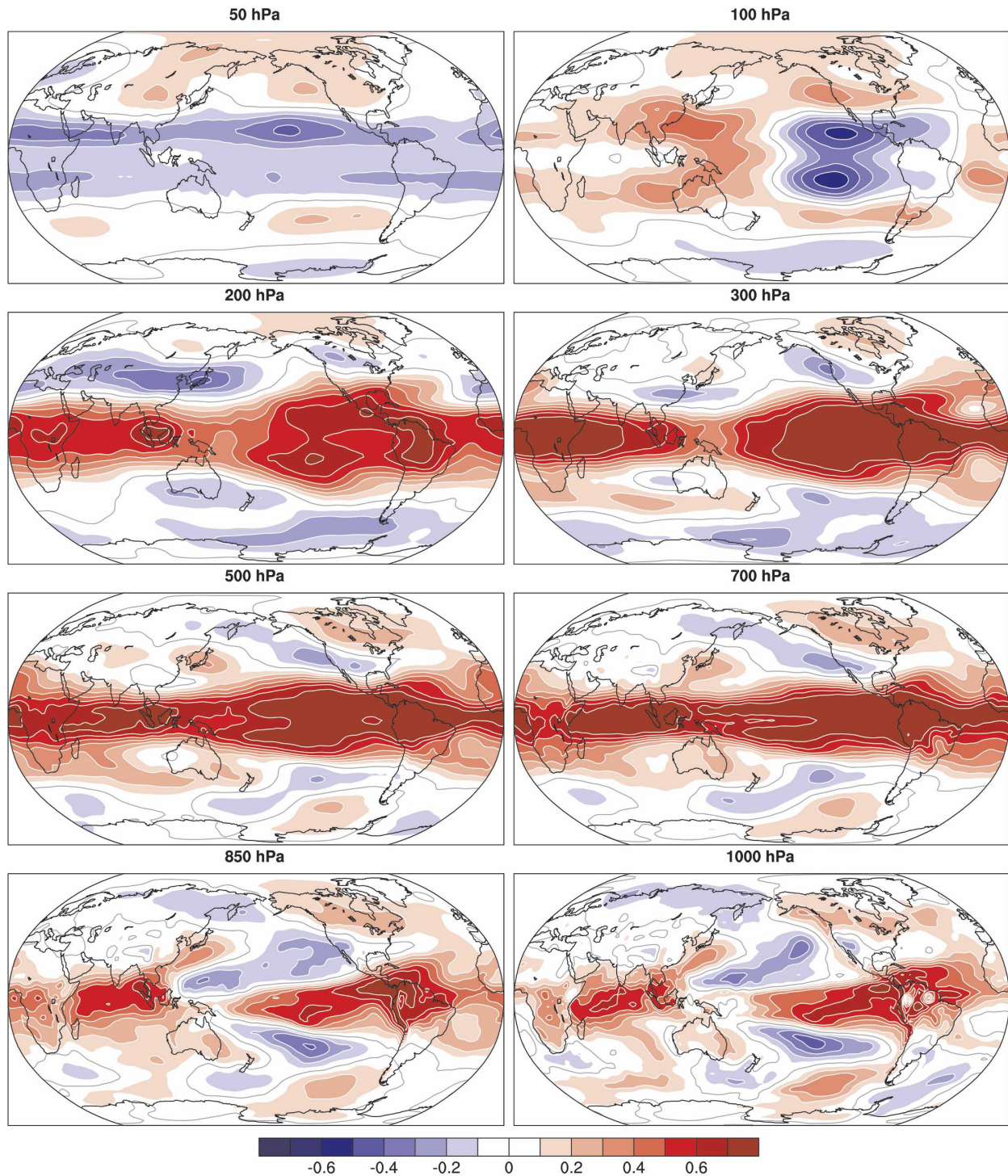
FIG. 6. For EOF-1: correlation maps at 1000, 850, 700, 500, 300, 200, 100, and 50 hPa.

1997/98 El Niño is evident with maximum warming in the tropical East Pacific at 1000 hPa, extending into the Atlantic and Indian Oceans (Trenberth et al. 2002a), although the warming in both those oceans is delayed relative to the Pacific. The characteristic boomerang-shaped cool anomalies in the western tropical Pacific, extending into the subtropics of the Pacific in both hemispheres, are also evident. So too are the Pacific−
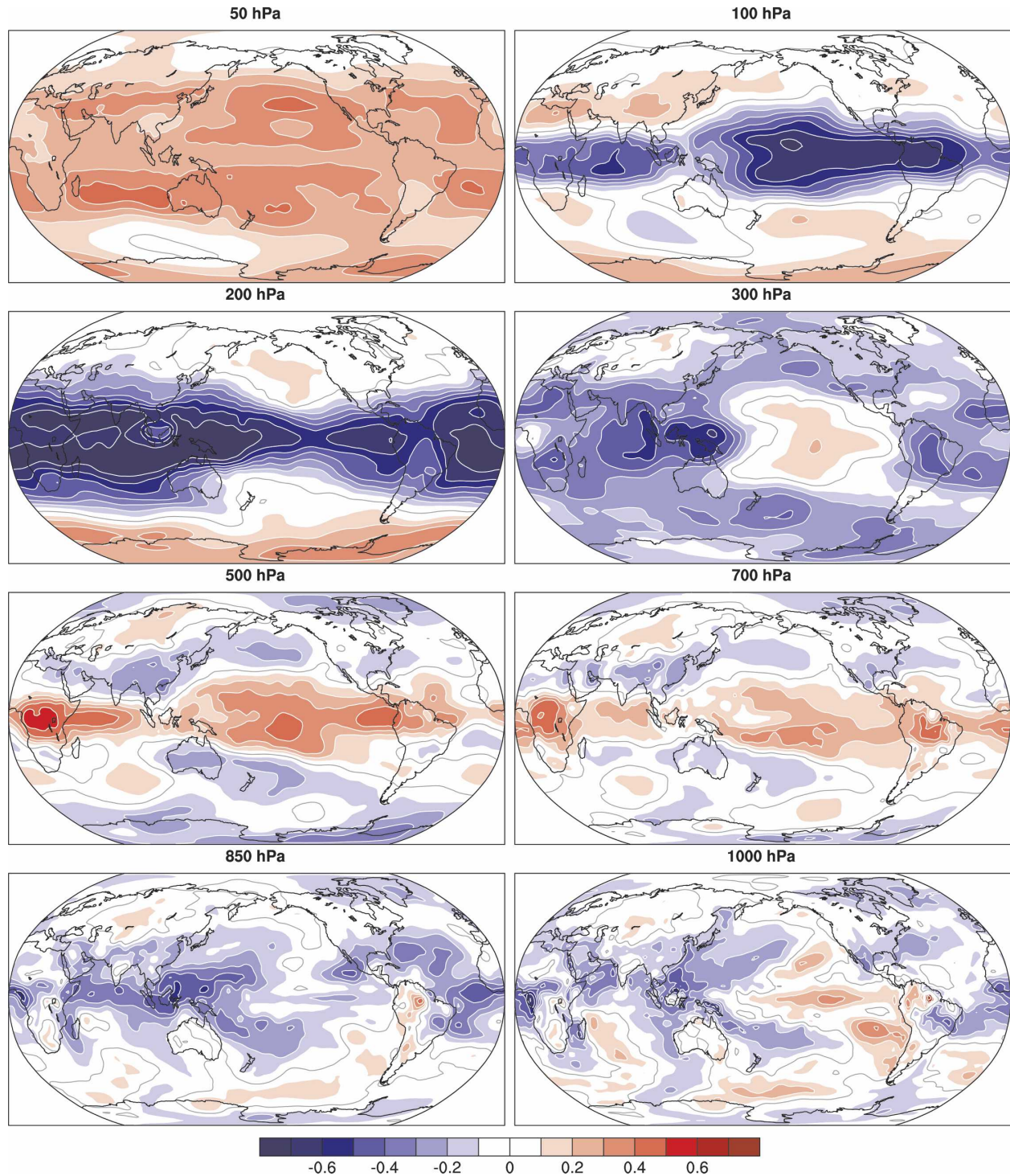
FIG. 7. For EOF-2: correlation maps at 1000, 850, 700, 500, 300, 200, 100, and 50 hPa.

North American wave structures and extensive warming over Canada, so that the absence of a zonal mean signal at higher latitudes is merely because the wave structures largely cancel. By 700 hPa, however, the warming is zonal in the Tropics, although with a maximum near the East Pacific, and at 200 hPa the characteristic off-equatorial Rossby wave maxima appear in the central Pacific. This reverses sign at 100 hPa, con-
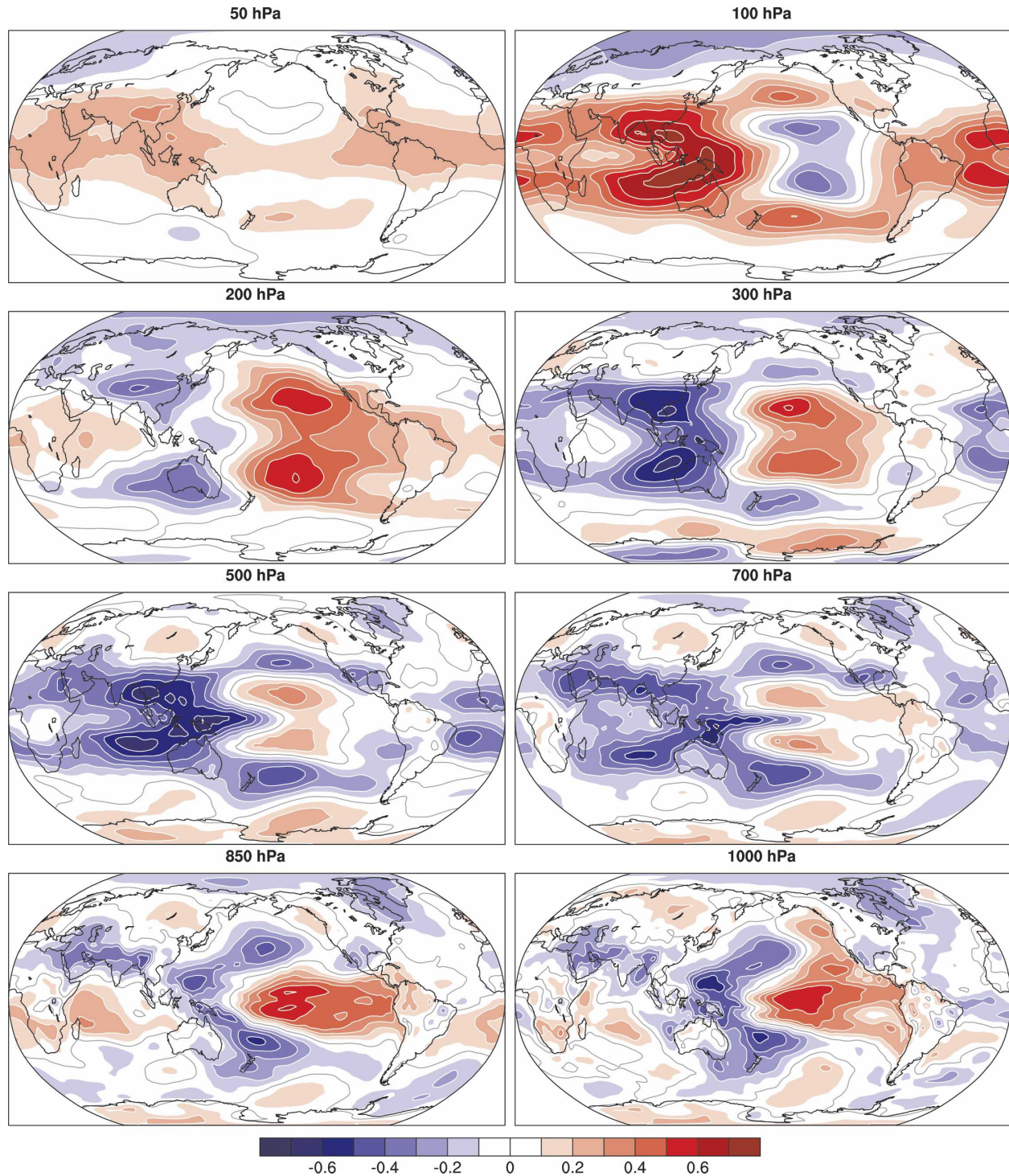
FIG. 8. For EOF-3: correlation maps at 1000, 850, 700, 500, 300, 200, 100, and 50 hPa.

sistent with a high tropopause. At 50 hPa the Tropics are cool but the extratropics are slightly warm and with a fairly zonal structure. Pattern correlations exceed 0.8 from 700 to 300 hPa in the tropical eastern Pacific–South American region.

Very different patterns exist for EOF-2. A weak El Niño structure is evident at 1000 hPa, but most of the Tropics has negative signs, which, given the downward trend in the time series, corresponds to warming throughout the period. The tropical warming at 700–

500 hPa is fairly zonally symmetric but at 300 hPa the Rossby wave structure straddling the equator is evident in the central Pacific as a warm anomaly, amidst much cooler conditions elsewhere. Cooling is evident in the Tropics at 200 and 100 hPa, and weak but widespread warming at 50 hPa. However by far the strongest pattern correlations are at 200 hPa, where they exceed –0.8 northwest of Australia.

The EOF-3 pattern at 1000 hPa has the tropical Pacific warming much broader than the other EOFs, extending north and south along the coasts of the Americas and well out of the Tropics. The cool boomerang dipole structure in the western Pacific is also well developed. Anomalies are small outside of the Pacific at 1000 and 850 hPa. The Rossby wave structures straddling the equator are very distinctive from 700 to 200 hPa, reversing in sign at 100 hPa, and with strong structures of opposite sign over the Maritime Continent near Indonesia at all these levels, forming a quadrupole. Modest warming prevails at 50 hPa. Pattern correlations exceed 0.75 near Indonesia at 100 hPa, although values are quite strong throughout the troposphere.

d. Relationships with indices

The indications from the above are that the ENSO events during this period are quite dissimilar in a number of ways when the full tropical structure is taken into account, which likely relates to overall warming and climate change, effects of volcanic events, and the different flavors of El Niño. We have therefore simply performed correlation analysis with a number of common climate or atmospheric circulation indices [see Table 1; Trenberth et al. (2005b) for a more complete discussion of the indices]. First, to dismiss several from further consideration, we note that none of the EOFs have significant correlations with the North Atlantic Oscillation (NAO), NAM, or SAM, highlighting their essentially tropical origins.

Monthly anomalies of EOF-1 with the SOI reveal maximum values at 3- and 4-month lags for EOF-1 of -0.56, or –0.43 at zero lag; and with the Niño-3.4 SST index it is 0.77 at a 4-month lag. This fits with the lead/lag relationships in Trenberth et al. (2002a) whereby the main temperature anomalies in tropical oceans outside the Pacific occur with a 5-month lag and overall global warming with El Niño occurs about 3 months after the peak in Niño-3.4 SSTs. Correlations with global mean surface temperatures (peak 0.42 lagging Niño-3.4 SSTs by 1 month for this period) are also highly significant.

EOF-2 and EOF-3 are both well correlated with the SOI and Niño-3.4 at zero lag with respective values of –0.29 and 0.30 for EOF-2 and –0.74 and 0.59 for EOF-3,

TABLE 1. Correlation between monthly anomaly EOF time series and climate indices for 1979–2001. Values in italics are statistically significant.

	Niño-3.4	SOI	TNI	NPI	50-hPa T	Global surface T
EOF-1	*0.58*	*−0.43*	*0.25*	−0.20	*−0.22*	*0.42*
EOF-2	*0.30*	−0.27	−0.02	−0.13	*0.37*	*−0.48*
EOF-3	*0.59*	*−0.68*	*−0.29*	−0.18	*0.21*	0.02

again confirming the relationship with ENSO but suggesting distinct differences in character. There is some hint that EOF-3 leads the ENSO indices by 1 to 2 months, as correlations are 0.61 and 0.60 at 1- and 2-month leads over Niño-3.4. EOF-2 has highest correlations with Niño-3.4 leading by 3 and 4 months (0.37), also suggesting some lags in the system. Moreover EOF-1 is correlated at -0.20 with the North Pacific index (NPI), and this increases substantially in magnitude to –0.42 when values are smoothed to emphasize interannual variations. The NPI is closely related to Pacific decadal variability (see Trenberth et al. 2005b). The second SST pattern of tropical variability related to the character of ENSO evolution is the TNI (Trenberth et al. 2002b), which also exhibits modest but significant correlations with EOF-1 and EOF-3, with indications that EOF-1 leads TNI by 3 to 4 months (0.33) and TNI leads EOF-3 by 5 months (-0.36).

All three EOFs have significant correlations with the tropical 50-hPa temperature mean time series (Fig. 2). Note that the EOF analysis did not include the 50-hPa level or else this relationship may be even more pronounced, but this suggests a nontrivial influence of both trends and perhaps volcanic eruptions in the EOFs. In particular, EOF-2 is strongly positively correlated with the 50-hPa T index at all leads and lags to ±5 months, maximum 0.40, minimum 0.31, suggesting that it is the trend that dominates this relationship. EOF-1 and EOF-2 both have highly significant correlations with global mean surface temperature.

To determine the sea level pressure and upper-tropospheric circulation fields associated with these patterns, we have regressed the time series onto the sea level pressure and 300-hPa geopotential height fields, shown for only EOF-1 and EOF-3 in Figs. 9 and 10. Both feature SO-like sea level pressure patterns but with important differences. For EOF-1 (Fig. 9) the east–west dipole structure is strongest in the equatorial region, as it was for the 1997/98 El Niño. The more classic SO structure with maximum correlations off the equator in the East Pacific and highest in the South Pacific, including the Tahiti area (see Trenberth and Caron 2000), is featured in EOF-3. The teleconnection
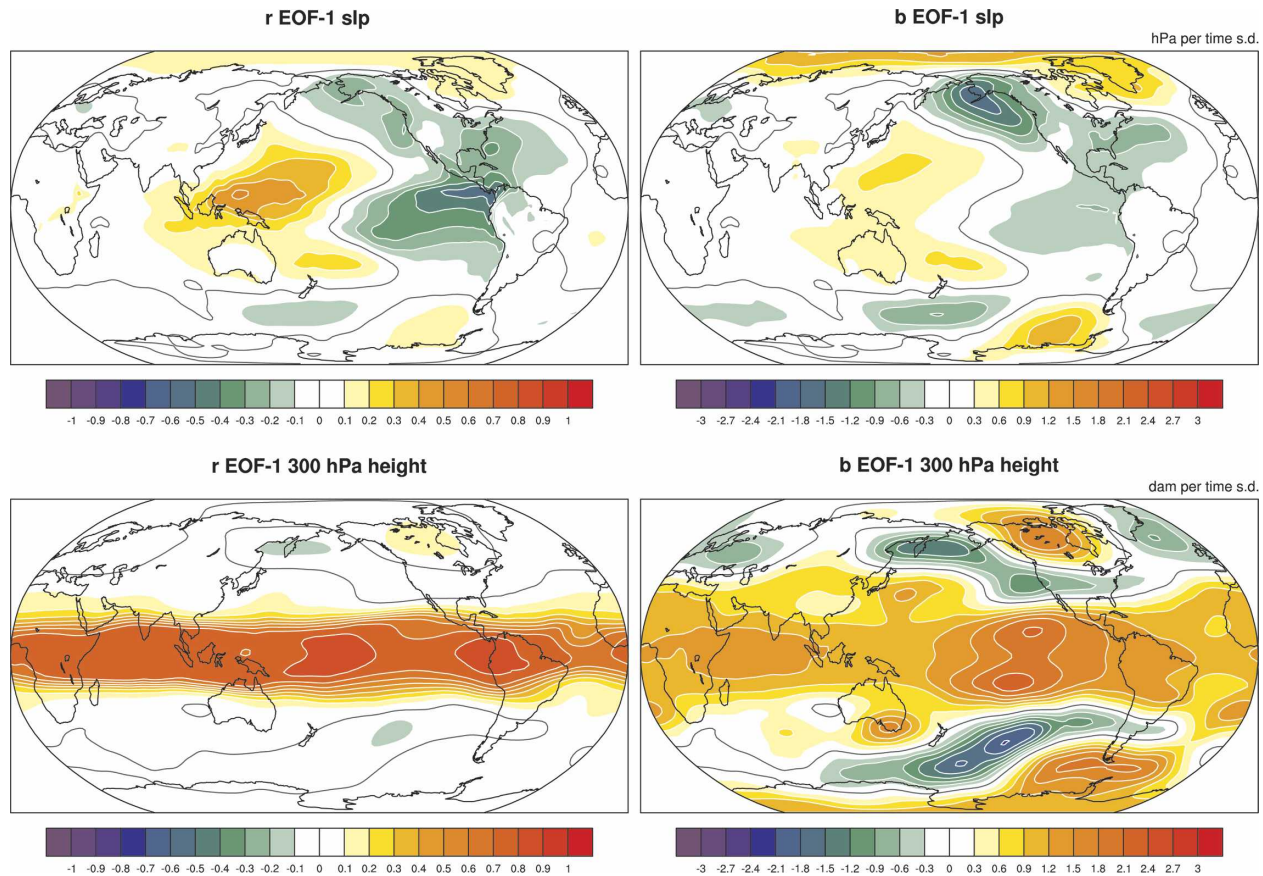
FIG. 9. Patterns of (left) correlation and (right) regression of EOF-1 with (top) sea level pressure and (bottom) 300-hPa height. The units at right are hPa or dam per standard deviation of the time series.

to the North Pacific is clear in both cases but with the EOF-1 pattern featuring an extension toward California, while the Pacific–North American teleconnection pattern is more evident in EOF-3. In the upper troposphere, EOF-1 becomes zonal and has high heights in the Tropics and strong maxima in the eastern Pacific straddling the equator, and teleconnection patterns downstream toward higher latitudes in both hemispheres, but is fairly weak. The extratropical teleconnections are more statistically significant and stronger for EOF-3, with major changes over the North Pacific and North American region, and are similar but more wave-like in the SH.

4. Discussion

There are some uncertainties in the ERA-40 reanalyses and how well they depict the true state of the atmosphere over the period 1979 to 2001. Problems with assimilation of satellite radiances at times of volcanic eruptions owing to aerosol contamination of the assumed relationships are known to exist (Uppala et al.

2005). Other problems also exist that seem to be reflected in EOF-2, as discussed below.

EOF-1 depicts ENSO in recent times, especially as seen in the 1997/98 El Niño event. It is strongly correlated with the ENSO indices and lags them by 3 to 4 months. As El Niño develops, the buildup of heat in the ocean spreads eastward across the Pacific and then poleward along the Americas within the ocean. At the same time, strong accompanying convection pumps heat into the atmosphere and drives teleconnections throughout the Tropics that extend to higher latitudes (Trenberth et al. 2002a,b). In the Tropics, the overturning atmospheric circulation creates subsidence and clear skies over the tropical Indian and Atlantic Oceans, which subsequently warm, and peak several months after Niño-3.4 SSTs. The general heating of the atmosphere also leads to a mini global warming that peaks, on average, three months after the peak in Niño-3.4 SSTs at the surface. EOF-1 captures much of this behavior. In the deep Tropics, it features an increase in amplitude of temperature perturbation with height, consistent with the dominant process of moist convec-
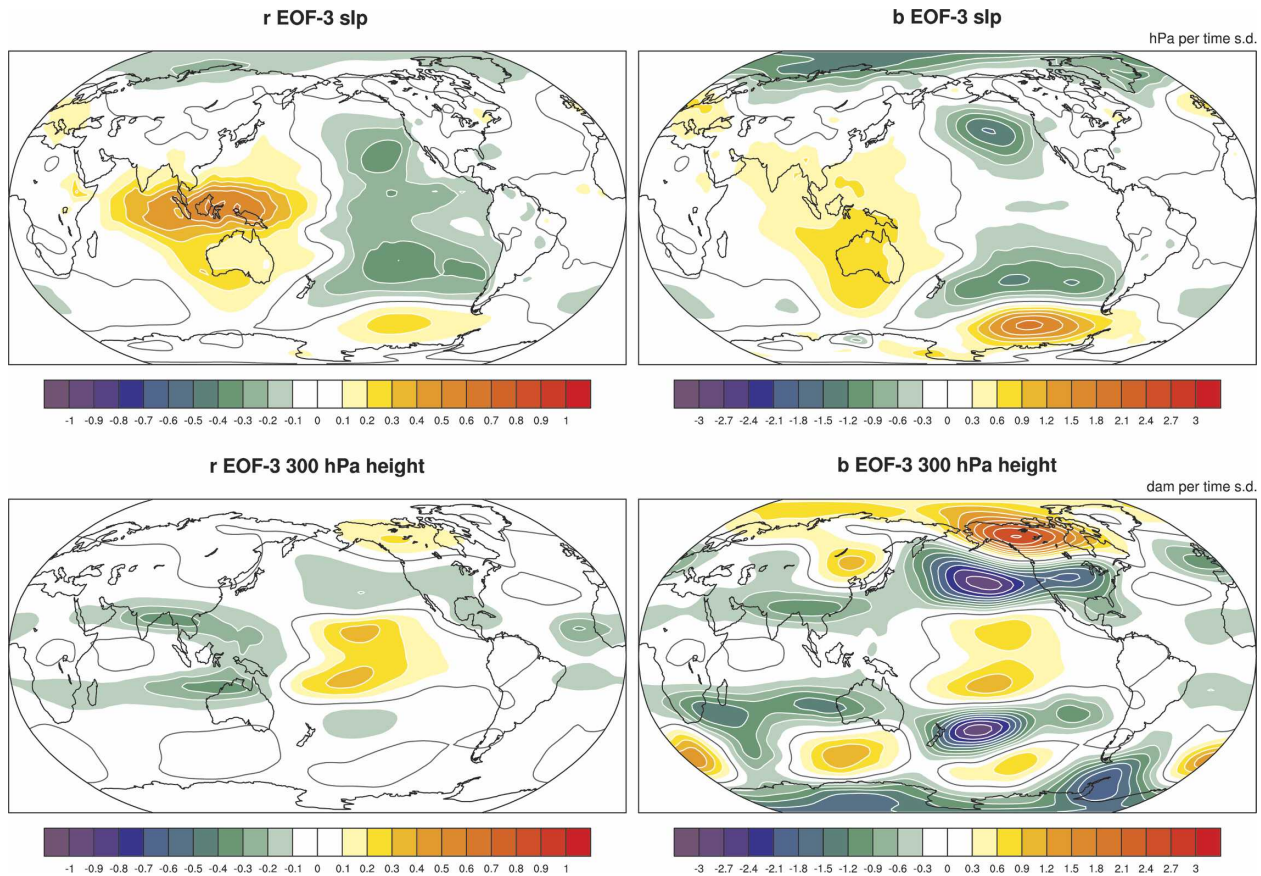
FIG. 10. Patterns of (left) correlation and (right) regression of EOF-3 with (top) sea level pressure and (bottom) 300-hPa height. The units at right are hPa or dam per standard deviation of the time series.

tion and the moist-adiabatic lapse rate, and as seen in models (Santer et al. 2005). The peak temperature magnitude is at 300 hPa and drops to zero at the tropopause. The temperature anomalies reverse sign in the lower stratosphere, also consistent with being driven from below but the signal is confined to below about 30 hPa. Regionally, the Rossby wave dipole response in the Pacific, reversing in sign at 100 and 50 hPa, is also consistent with previous understanding and model results.

EOF-2 is dominated by an overall trend. Indeed, when linear temperature trends averaged over the Tropics are computed for 1979–2001, they are positive from 1000 to 775 hPa, negative from 700 to 400 hPa, positive for 300 to 100 hPa with large values exceeding $1°C$ for the entire period at 200 and 150 hPa, and then negative trends at and above 70 hPa. This strange vertical structure of linear trends is manifested in EOF-2. At the same time, surface temperatures have generally trended upward during this time, both globally and in the Tropics, while temperatures in the lower stratosphere have generally declined, although punctuated by

the volcanic eruption warmings. All of these factors contribute to EOF-2. The surface and stratospheric trends and volcanic signals are real. The most puzzling aspect is the reversal in sign of trends in the troposphere from 700 to 400 hPa, which arises from a prolonged pronounced warming from 1979 to 1983 that is out of character with the rest of the record. At these levels the time series looks much like that for EOF-2. Such a warming feature is not present at all in the National Centers for Environmental Prediction–National Center for Atmospheric Research (NCEP–NCAR) reanalyses at 500 hPa, for instance (see Fig. 11 of Simmons et al. 2004), and therefore must be questioned. The negative trends are largest over the eastern tropical Pacific, Africa, and part of the Indian Ocean, where they are dependent primarily on satellite data.

Previous studies have found evidence of problems in MSU channel 3, which peaks near 300 hPa in terms of its vertical weighting function, and the evidence suggests spurious drifts for National Oceanic and Atmospheric Administration (NOAA) satellites *NOAA-6* and *NOAA-9* (e.g., Spencer and Christy 1992). In the

15-yr ECMWF Re-Analysis (ERA-15) problems were encountered in November 1986 when tropospheric temperatures exhibited a sudden jump caused by a shift in radiances from the MSU-3 channel on the *NOAA-9* polar-orbiting satellite following a cosmic storm, so they became warmer in the lower troposphere and colder in the upper troposphere. This was especially apparent in the Tropics. The effects were perpetuated in later ERA-15 analyses by the bias correction (Trenberth et al. 2001).

Although the ERA-15 problem is avoided in ERA-40 by blacklisting those data, MSU channel-3 radiances from *NOAA-6* were used in ERA-40 from June 1979 to April 1983 and again mainly from November 1985 to October 1986. Moreover, Simmons et al. (2004) have identified the 1979 to 1982 period as problematic for tropical temperature bias in ERA-40 (see their Fig. 11), likely due to poor bias correction of early TOVS data, and the structure may have arisen in part from structure functions in the data assimilation system, especially from the Stratospheric Sounder Unit (A. J. Simmons 2005, personal communication). Santer et al. (2004) discuss some problems with ERA-40 temperatures, but the problems revealed here may have affected their analysis of trends in tropopause height.

EOF-3, however, depicts an alternative temperature structure to that in EOF-1 for ENSO and highlights the sequence of three successive El Niño events in the early 1990s. It features decadal variability and somewhat longer time scales, and much broader structures meridionally in the Pacific, as previously identified with Pacific decadal variability (Zhang et al. 1997; Garreaud and Battisti 1999). This pan-Pacific pattern is dominated by Southern Oscillation wave-1 structures throughout the Tropics and subtropics and has strongest values in the Pacific but extending well into the extratropics. Strong Rossby wave signatures are featured in the troposphere with a distinctive quadrupole pattern that reverses at 100 hPa. It features zonal mean warming below 700 hPa, cooling from 700 to 300 hPa, and warming above, peaking at 100 hPa and extending from 40°N to 50°S, but these are seen to be small residuals of the stronger regional patterns, and there is no contribution to global mean surface values.

The vertical coherence of all patterns suggests that they should be apparent in broad-layer satellite temperature records. MSU channel 2, for instance, would depict EOF-1 quite well but would not capture the physically associated reversal in sign in the lower stratosphere. However, MSU channel 4 in the lower stratosphere is ideally structured to pick that up, and so the Fu technique (Fu et al. 2004a) of combining MSU channels 2 and 4 is essential in depicting the EOF-1 struc-

ture. For EOF-3, broad vertical structures are again present but with the transition around 300 hPa, so that it is not much influenced by MSU channel 3. MSU channel 4 should nonetheless represent the region above there, as it is coherent through 30 hPa. A key point is that the stratosphere generally has the opposite sign to the troposphere, and so while it may be possible to treat these as separate regions, they are in fact strongly physically linked.

In EOF-2, the structure in the troposphere is likely spurious, with spurious cooling near 500 hPa and too much warming in the upper troposphere. It projects much more strongly onto MSU channel 3 than either of the other EOFs. However, even for this pattern, the stratosphere above 100 hPa has opposite sign to that in the upper troposphere and surface. Surface SST–related temperature trends should probably be coherent throughout the troposphere, although stratospheric influences from ozone depletion or aerosol heating may be much more limited in vertical extent.

Not shown here are the hemispheric or seasonal results from EOF analyses (section 2). Trenberth et al. (2005b) found that such stratification of the data is desirable to better depict the changing patterns with season and focus on extratropical patterns from the NAO, NAM, and SAM, and seasonal changes in tropical teleconnections. However, as the pervasive global influence of ENSO dominates results, we have focused on those aspects here as it is essential to recognize the different spatial and vertical temperature structures accompanying similar sea level pressure patterns given by the SOI.

5. Conclusions

The dominance of ENSO in global and tropical variability makes it unsurprising that it dominates the first temperature EOF, but the analysis highlights the fact that there are different flavors of El Niño when the full three-dimensional structure of the atmospheric circulation and temperature field is considered, and more than one EOF is essential to capture the full character of ENSO. EOF-1 captures the 1997/98 El Niño event, and this pattern projects onto most other events as well, with the important exception of the ENSO events in the early 1990s. But EOF-3 is also important, especially for the lower frequencies, and is likely more important for most moderate or weak El Niño events. Thus while the sea level pressure patterns have similarities, the vertical structures differ considerably.

In this study we analyzed the vertical temperature structure in the monthly mean anomalies from ERA-40 for a core region of the Tropics from 30°N to 30°S, but

with results projected globally. The first three EOFs feature rather different vertical structures. EOF-2 dominates the temperature trends in the Tropics and has a very complex vertical structure that apparently arises from problems with bias adjustment in assimilating satellite data. The evidence suggests that it is not real, although it captures some real trends associated with global surface warming and stratospheric cooling.

The dominant pattern (EOF-1) in its positive sign, features highly coherent zonal mean warming throughout the tropical troposphere from 30°N to 30°S that increases in magnitude with height to 300 hPa, drops to zero at about 100 hPa at the tropopause, and has reverse sign to 30 hPa with peak negative values at 70 hPa. Warmth dominates throughout most of the Tropics although with opposite anomalies in the western tropical Pacific (weak) and Pacific subtropics (strong). Coherent wave structures at higher latitudes cancel out in the zonal mean. The structure is more zonal above about 700 hPa and features off-equatorial maxima straddling the equator in the eastern Pacific in the upper troposphere with opposite sign at 100 hPa, as a signature of a forced Rossby wave. It plays a dominant role in the 1997/98 El Niño and is also featured in 1982/83 and 1986/87 events, and the 1988/89 La Niña. It is followed a few months later by an increase in global mean surface temperatures.

EOF-3 picks up the lower-frequency ENSO decadal variation and corresponds more closely with the traditional SO. In the zonal mean it features weak warming below 700 hPa, cooling from 700 to 300 hPa, and warming above that level that peaks at 100 hPa and extends from 40°N to 50°S. However, the zonal mean is a residual of a much stronger wave pattern that changes sign across about the date line and is fairly coherent throughout the troposphere from the surface through 200 hPa, reversing in sign at 100 hPa. Strong Rossby wave signatures are featured in the troposphere with a distinctive quadrupole pattern that reverses at 100 hPa.

The vertical coherence of all patterns suggests that they should be apparent in broad-layer MSU satellite temperature records but that the accompanying stratospheric signature has opposite sign. Consequently, individual MSU channels are not optimal for monitoring temperature of the atmosphere, and contributions from two or more channels (cf. Fu et al. 2004a) are required. Similarly, boxcar weights of a single tropospheric layer may not be optimal as they would be negatively correlated with stratospheric values. The quite different three-dimensional structure of these different ENSO patterns highlights the need to consider the full structure outside of the Pacific and at all levels in ENSO and the relationship to the global mean. The changes in atmospheric circulation and associated changes in storm tracks would be different, for instance, across North America, depending on which pattern dominates. However, trends are not reliably depicted in ERA-40 and in this analysis.

REFERENCES

Bromwich, D. H., and R. L. Fogt, 2004: Strong trends in the skill of the ERA-40 and NCEP–NCAR reanalyses in the high and middle latitudes of the Southern Hemisphere, 1958–2001. *J. Climate,* **17,** 4603–4619.

Christy, J. R., R. W. Spencer, and W. D. Braswell, 2000: MSU tropospheric temperatures: Dataset construction and radiosonde comparisons. *J. Atmos. Oceanic Technol.,* **17,** 1153–1170.

——, ——, W. B. Norris, W. D. Braswell, and D. E. Parker, 2003: Error estimates of version 5.0 of MSU/AMSU bulk atmospheric temperatures. *J. Atmos. Oceanic Technol.,* **20,** 613–629.

Free, M., J. K. Angell, I. Durre, J. Lanzante, T. C. Peterson, and D. J. Seidel, 2004: Using first differences to reduce inhomogeneity in radiosonde temperature datasets. *J. Climate,* **17,** 4171–4179.

——, D. J. Seidel, J. K. Angell, J. Lanzante, I. Durre, and T. C. Peterson, 2005: Radiosonde atmospheric temperature products for assessing climate (RATPAC): A new dataset of large-area anomaly time series. *J. Geophys. Res.,* **110,** D22101, doi:10.1029/2005JD006169.

Fu, Q., and C. M. Johanson, 2004: Stratospheric influence on MSU-derived tropospheric temperature trends: A direct error analysis. *J. Climate,* **17,** 4636–4640.

——, and ——, 2005: Satellite-derived vertical dependence of tropical tropospheric temperature trends. *Geophys. Res. Lett.,* **32,** L10703, doi:10.1029/2004GL022266.

——, ——, S. G. Warren, and D. J. Seidel, 2004a: Contribution of stratospheric cooling to satellite-inferred tropospheric temperature trends. *Nature,* **429,** 55–58.

——, D. J. Seidel, C. M. Johanson, and S. G. Warren, 2004b: Stratospheric cooling and the troposphere (reply). *Nature,* **432,** doi:10.1038/nature03210.

Garreaud, R. D., and D. S. Battisti, 1999: Interannual and interdecadal variability of the tropospheric circulation in the Southern Hemisphere. *J. Climate,* **12,** 2113–2123.

Jones, P. D., and A. Moberg, 2003: Hemispheric and large-scale surface air temperature variations: An extensive revision and an update to 2001. *J. Climate,* **16,** 206–223.

Mears, C. A., M. C. Schabel, and F. J. Wentz, 2003: A reanalysis of the MSU channel 2 tropospheric temperature record. *J. Climate,* **16,** 3650–3664.

Randel, W. J., and F. Wu, 2006: Biases in stratospheric and tropospheric temperature trends derived from historical radiosonde data. *J. Climate,* **19,** 2094–2104.

Rayner, N. A., D. E. Parker, E. B. Horton, C. K. Folland, L. V. Alexander, D. P. Rowell, E. C. Kent, and A. Kaplan, 2003:

Global analyses of sea surface temperature, sea ice, and night marine air temperature since the late nineteenth century. *J. Geophys. Res.,* **108,** 4407, doi:10.1029/2002JD002670.

Robock, A., 2002: Volcanic eruption, El Chichon. *The Earth System: Physical and Chemical Dimensions of Global Environmental Change,* M. C. MacCracken and J. S Perry, Eds., Encyclopedia of Global Environmental Change, Vol. 1, John Wiley and Sons, 736–736.

Santer, B. D., J. J. Hnilo, T. M. L. Wigley, J. S. Boyle, C. Doutriaux, M. Fiorino, D. E. Parker, and K. E. Taylor, 1999: Uncertainties in observationally based estimates of temperature change in the free atmosphere. *J. Geophys. Res.,* **104,** 6305–6333.

——, and Coauthors, 2004: Identification of anthropogenic climate change using a second-generation reanalysis. *J. Geophys. Res.,* **109,** D21104, doi:10.1029/2004JD005075.

——, and Coauthors, 2005: Amplification of surface temperature trends and variability in the tropical atmosphere. *Science,* **309,** 1551–1556.

Seidel, D. J., and Coauthors, 2004: Uncertainty in signals of large-scale climate variations in radiosonde and satellite upper-air temperature datasets. *J. Climate,* **17,** 2225–2240.

Sherwood, S., J. Lanzante, and C. Meyer, 2005: Radiosonde daytime biases and late 20th century warming. *Science,* **309,** 1556–1559.

Simmons, A. J., and Coauthors, 2004: Comparison of trends and low-frequency variability in CRU, ERA-40, and NCEP/NCAR analyses of surface air temperature. *J. Geophys. Res.,* **109,** D24115, doi:10.1029/2004JD005306.

Spencer, R. W., and J. R. Christy, 1992: Precision and radiosonde validation of satellite gridpoint temperature anomalies. Part II: A tropospheric retrieval and trends during 1979–90. *J. Climate,* **5,** 858–866.

Tett, S. F. B., and P. W. Thorne, 2004: Tropospheric temperature series from satellites. *Nature,* **429,** doi:10.1038/nature03208.

Thorne, P. W., D. E. Parker, S. F. B. Tett, P. D. Jones, M. McCarthy, H. Coleman, and P. Brohan, 2005: Revisiting radiosonde upper air temperatures from 1958 to 2002. *J. Geophys. Res.,* **110,** D18105, doi:10.1029/2004JD005753.

Trenberth, K. E., and T. J. Hoar, 1996: The 1990–1995 El Niño Oscillation event: Longest on record. *Geophys. Res. Lett.,* **23,** 57–60.

——, and ——, 1997: El Niño and climate change. *Geophys. Res. Lett.,* **24,** 3057–3060.

——, and J. M. Caron, 2000: The Southern Oscillation revisited: Sea level pressures, surface temperatures, and precipitation. *J. Climate,* **13,** 4358–4365.

——, and D. P. Stepaniak, 2001: Indices of El Niño evolution. *J. Climate,* **14,** 1697–1701.

——, ——, J. W. Hurrell, and M. Fiorino, 2001: Quality of reanalyses in the Tropics. *J. Climate,* **14,** 1499–1510.

——, J. M. Caron, D. P. Stepaniak, and S. Worley, 2002a: Evolution of El Niño–Southern Oscillation and global atmospheric surface temperatures. *J. Geophys. Res.,* **107,** 4065, doi:10.1029/2000JD000298.

——, D. P. Stepaniak, and J. M. Caron, 2002b: Interannual variations in the atmospheric heat budget. *J. Geophys. Res.,* **107,** 4066, doi:10.1029/2000JD000297.

——, J. Fasullo, and L. Smith, 2005a: Trends and variability in column integrated atmospheric water vapor. *Climate Dyn.,* **24,** 741–758.

——, D. P. Stepaniak, and L. Smith, 2005b: Interannual variability of the patterns of atmospheric mass distribution. *J. Climate,* **18,** 2812–2825.

Uppala, S. M., and Coauthors, 2005: The ERA-40 reanalysis. *Quart. J. Roy. Meteor. Soc.,* **131,** 2961–3012.

Zhang, Y., J. M. Wallace, and D. S. Battisti, 1997: ENSO-like interdecadal variability: 1900–93. *J. Climate,* **10,** 1004–1020.